Available online at www.sciencedirect.com
ScienceDirect
Journal of Power Sources 177 (2008) 111–122
JOURNAL OF POWER SOURCES
www.elsevier.com/locate/jpowsour

Experimental investigations of the microscopic features and polarization limiting factors of planar SOFCs with LSM and LSCF cathodes

P. Leone, M. Santarelli *, P. Asinari, M. Calì, R. Borchiellini

Dipartimento di Energetica, Politecnico di Torino, Corso Duca degli Abruzzi 24, 10129 Torino, Italy

Received 31 July 2007; received in revised form 1 November 2007; accepted 4 November 2007
Available online 17 November 2007

Abstract

The paper deals with the microscopic and polarization evaluation of planar circular-shaped seal-less SOFC cells from InDEC® with an outline of performance limiting factors at reduced temperature. The cells consist of porous NiO–YSZ anode as mechanical support, NiO–YSZ anode active layer, yttria-stabilized zirconia (YSZ) electrolyte, and only differ for the cathode design. A first design (ASC1) with strontium doped lanthanum manganate LSM–YSZ cathode functional layer (CFL) and LSM cathode current collector layer (CCCL); the second design (ASC2) with yttria doped ceria (YDC) barrier layer and lanthanum strontium cobalt ferrite oxide (LSCF) cathode.

The microscopic analysis was performed using SEM methods. The electrical characterization was performed by taking current–voltage measurements over a range of temperatures between 650 and 840 °C with hydrogen as fuel, and air as oxidant.

The analysis of performance showed that at 740 °C the voltage of 700 mV is reached at around a double value of current density in the case of ASC2. Further, the dependence of performance on the various polarization contributions was rationalized on the basis of an analytical model. Through a parameter estimation on the experimental data, it was possible to determine some polarization parameters for the two cells such as the effective exchange current densities, ohmic resistance and anodic limiting current density.

It is shown that the performance limitation at low temperature is due to activation polarization for ASC1 and ohmic polarization for ASC2. Based on the results of the investigation, it is concluded that LSCF cathodes are really effective for decreasing the cathode activation polarization, allowing the reduction of operating temperature.
© 2007 Elsevier B.V. All rights reserved.

Keywords: Planar SOFCs; Polarization; Microscopy analysis; Cathodes; LSM; LSCF

1. Introduction

An experimental analysis on planar anode-supported SOFC cells is presented. The test sessions were performed at the IN.TE.SE laboratory of the Department of Energy of the Politecnico di Torino, where a test facility for testing planar SOFCs is installed. The results concern the characterization of anode-supported cells with LSM and LSCF cathodes. The analysis focused on the characterization of the cell performances according to the different cathode design. The experimental data analysis consisted in the definition and evaluation of performance indexes of cells such as maximum power density, current density at 700 mV, area specific resistance (ASR) analysis and polarization analysis coupled with parameter estimation methods. The principal aim is to outline the limiting factors of the two different structures at reduced temperature [1–11].

The understanding of the analysed data required a deep overview of literature concerning the main features of cathodes based on composite and mixed electronic and ionic conductors (MEIC) materials.

Lanthanum–strontium manganite (LSM) is recognized as a promising candidate for SOFC cathode in real applications, due to mechanical and chemical compatibility with zirconia electrolyte and good electrochemical performances at high temperatures. However, its polarization property at low temperatures (≤800 °C) is not satisfactory.

The medium-temperature performance can be enhanced when a second ionic conducting phase is added to LSM to extend the active surface over which the oxygen reduction reaction can occur: very good results were obtained using a LSM–YSZ

* Corresponding author. Tel.: +39 011 090 4487; fax: +39 011 090 4499.
E-mail address: massimo.santarelli@polito.it (M. Santarelli).

0378-7753/$ – see front matter © 2007 Elsevier B.V. All rights reserved.
doi:10.1016/j.jpowsour.2007.11.021

Nomenclature

ASR	area specific resistance ($\Omega\,cm^2$)
B	grain size of the electrolyte in the composite electrode (cm)
E_a	thermal activation energy (eV)
F	Faraday number ($C\,mol^{-1}$)
h	electrode functional layer thickness (cm)
i	cell current density ($A\,cm^{-2}$)
i_{as}	anode limiting current ($A\,cm^{-2}$)
i_{cs}	cathode limiting current ($A\,cm^{-2}$)
$I_{0,c}$	effective exchange current density ($A\,cm^{-2}$)
LSCF	lanthanum strontium cobalt ferrite oxide
LSM	lanthanum strontium manganese oxide
MPD	maximum power density ($mW\,cm^{-2}$)
OCV_{exp}	open circuit voltage (V)
R	universal gas constant ($J\,mol^{-1}\,K^{-1}$)
R_c	cathode polarization resistance ($\Omega\,cm^2$)
R_{ct}	intrinsic charge transfer resistance ($\Omega\,cm^2$)
R_Q	Cell ohmic resistance ($\Omega\,cm^2$)
R_{YSZ}	ohmic electrolyte resistance ($\Omega\,cm^2$)
R_{ct}^{eff}	effective charge transfer resistance ($\Omega\,cm^2$)
SOFC	solid oxide fuel cell
T	temperature (K)
t_a	thickness of the anode layer (cm)
t_c	thickness of the cathode layer (cm)
V_c	cell terminal voltage (V)
V_{diff}	diffusion overpotential (V)
V_{Nernst}	Nernst potential (V)
YDC	yttria doped ceria
YSZ	yttria-stabilized zirconia

Greek letters

α	effective charge transfer coefficient
ε	electrode porosity
ρ_{el}	resistivity of electrolyte ($\Omega\,cm$)
σ_{8YSZ}	conductivity of electrolyte ($S\,cm^{-1}$)
τ	electrode tortuosity

cathode, but it is not clear the temperature reduction allowable by this structure depending mainly on the optimization of the microstructure. The composite electrode provides parallel paths for oxygen ions (through the electrolyte), electrons (through LSM) and gaseous species (through the pores). The composite electrode effectively increases the active surface area interfacing with the electrolyte, spreading it over the whole layer thickness. Iron and cobalt-containing perovskites (LSCF) are other candidates for SOFC cathode materials, because of their high electronic and ionic conductivity as well as high oxygen permeability and high electrocatalytic activity.

It is important to note that in the case of cathodes using pure electronic conducting materials (as lanthanum–strontium manganite) the electrochemical reactions are almost restricted to the triple phase boundary between the electronic conducting material, the ionic conducting material (electrolyte) and the gaseous oxygen. On the other side, LSCF cathodes, referred as mixed electronic and ionic conductors (MEIC), have appreciable ionic conductivity, and reduction of oxygen occurs at the electrode surface with diffusion of oxygen ions through the mixed conductor [12,13]. Nevertheless, LSCFs cathodes have to be selected carefully because they have a significantly higher thermal expansion coefficient (TEC) than the commonly used 8YSZ electrolyte ($\alpha_{YSZ} = 10.8 \times 10^{-6}\,K^{-1}$ (30–1000 °C) and in principle this mismatch can lead to degradation phenomena during thermal cycles, like delamination of the electrode layer. According to the lanthanum content the values found in literature are $17.1 \times 10^{-6}\,K^{-1}$ (30–1000 °C) for L55SCF, $17.4 \times 10^{-6}\,K^{-1}$ (30–1000 °C) for L58SCF, $13.8 \times 10^{-6}\,K^{-1}$ (30–1000 °C) for L78SCF [12]. Furthermore, this type of perovskite tends to react easier with zirconia electrolyte than LSM at high temperatures and the resulting $La_2Zr_2O_7$ or $SrZrO_3$ compounds have a higher ohmic resistivity. To overcome these problems, an interlayer consisting of $Ce_{0.8}Gd_{0.2}O_{2-\delta}$ (CGO) between cathode and electrolyte is often used [14].

Another physical property to consider is the electrical behavior of these materials. The electrical properties of YSZ and LSM are discussed in Ref. [15]. The LSM electrical conductivity is reported to be $3.5\,S\,cm^{-1}$ at 1000 °C and $2.08\,S\,cm^{-1}$ at 200 °C with an activation energy of $9.6\,kJ\,mol^{-1}$ (extrapolated from Arrhenius plot of experimental conductivities). Since this material is recognized as only an electronic carrier, the electrical conductivity expresses the electronic conductivity. For the 8YSZ the electrical conductivity is reported as $6.67 \times 10^{-2}\,S\,cm^{-1}$ at 1000 °C with much higher activation energy, equal to $93\,kJ\,mol^{-1}$. As before, the 8YSZ is only an ionic conductor and its electrical conductivity has to be considered as its ionic conductivity.

The CGO material has a higher ionic conductivity of 8YSZ in the composition $(CeO_2)_{0.8}(Gd_2O_3)_{0.2}$, especially at temperatures below 800 °C. At 700 °C its ionic conductivity is reported by Mogensen et al. to be $3.6 \times 10^{-2}\,S\,cm^{-1}$ with activation energy of $70\,kJ\,mol^{-1}$ [16].

Significant improvement in cell performance can be achieved by investigating new cathodes' materials [14,17–23]. In comparison with the performance of a state-of-the-art LSM/YSZ composite cathode, the current densities of the better performing LSCFs (L55SCF, L58SCF, L78SCF) are up to two times higher. Further, LSCF cathodes gave a power output of 1.0–1.2 $W\,cm^{-2}$ at 800 °C and 0.7 V with hydrogen as fuel gas: compared with conventional cathodes based on LSM, the high power densities allow a reduction in operating temperature of about 100 °C by maintaining the same performance [14]. In Ref. [17] the same authors compare performances of two cathode materials ($La_{0.58}Sr_{0.4}Co_{0.2}Fe_{0.8}O_{3-\delta}$ and $La_{0.8}Sr_{0.2}Co_{0.2}Fe_{0.8}O_{3-\delta}$). The cathode with $La_{0.58}$ gives the better result in terms of electrochemical performance. However, the thermal expansion coefficient also increases with higher Sr content, which can cause mechanical problems.

In Ref. [18] $La_{0.6}Sr_{0.4}Co_{0.2}Fe_{0.8}O_3$ (LSCF) and LSCF–$Ce_{0.8}Gd_{0.2}O_3$ (CGO) cathodes on YSZ electrolytes were studied for potential applications in low-temperature SOFC. The LSCF electrodes yielded low-current interfacial resistance

values that were a factor of 10 lower than for (La,Sr)MnO_3 cathodes. The addition of 50 vol.% CGO to LSCF resulted in an additional decrease factor of 10 in the polarization resistance. The fact is that even if LSCF has good ionic conductivity, its electronic conductivity is much more relevant. So adding to this material another MIEC material, such as CGO, which has a high ionic conductivity, is effective in increasing the overall ionic conductivity of the composite electrode LSCF/CGO. In Ref. [19] the cathode polarization curves of $Ln_{0.4}Sr_{0.6}Co_{0.8}Fe_{0.2}O_{3-\delta}$ (Ln = La, Pr, Nd, Sm, Gd) are shown. $Nd_{0.4}Sr_{0.6}Co_{0.8}Fe_{0.2}O_{3-\delta}$ exhibits the best catalytic activity for oxygen reduction. The electrical conductivity of these systems increases with temperature and reaches a maximum, and then decreases with a further increase in temperature. The conductivity values of all the compositions are higher than 100 S cm^{-1} above 600 °C, acceptable as a cathode in SOFC.

The overpotential of LaSrCOFeO cathode at 0.5 A cm^{-2} is around 100 mV at 800 °C and slightly more than 200 mV at 700 °C. The overpotential of LSM at 1000 °C and 0.5 A cm^{-2} is around 200 mV [20,21] while at 800 °C is around 700 mV [21].

The effect of adding a porous second ionic conducting phase to pure LSM lead to a decrease in the polarization resistance. For pure LSM a polarization resistance from 9 to 54 Ω cm^2 at 700 °C has been reported; with the addition of 50% YSZ phase in the LSM electrode, the polarization resistance of the LSM/YSZ composite cathode was reduced to 2.5 Ω cm^2 at 700 °C. The resistance was further reduced to 1.1 Ω cm^2 at 700 °C by substituting YSZ with high ionic conducting CGO phase in the LSM/CGO composite electrode [21].

In Ref. [22] the authors investigate the effect of adding thin porous yttria doped ceria (YDC) layers on either side of a YSZ electrolyte: much-reduced interfacial resistances at both LSM cathodes and Ni–YSZ anodes were found. In particular, cells with LSM cathodes with and without YDC interlayers were tested and compared: at each temperature, cells with YDC cathode interlayers yielded approximately five times higher power densities and an estimated decrease of cathode resistance of 10 times due to YDC. The YDC apparently provide a higher oxygen surface-exchange coefficient being a mixed conductor material. In particular YDC has a higher ionic conductivity compared to 8YSZ at temperature below 800 °C, in fact at 700 °C its conductivity is around 0.01 S cm^{-1} [2].

In Ref. [23] a screening of different cathode properties for application in low-temperature SOFC technology is presented: basing on impedance spectroscopy analysis on symmetrical cells it was found a polarization resistance of 0.5 Ω cm^2 for LSM cathode at around 760 °C, at 700 °C for LaSrFeCu, at 650 °C for LaSrFeCo, at 580 °C for SrFeCo and 550 °C for PrSrCo. These materials, even being promising from an electrochemical point of view, have still to show their chemical compatibility with the common used electrolyte materials (YSZ, CGO) and the continuity of their performances after several working hours. At the moment LSM is still the best candidate for producing commercial or pre-commercial devices. As shown in this paper, cells with composite LSM/8YSZ has good performance, but not brilliant anyway. In fact, the use of LSCF as cathode material for SOFCs effectively enhances the performance of the cell and allows one the reduction of the operating temperature. Moreover, the work focused on the polarization limiting factors during the reduction of the operating temperature (range 740–840 °C). In the cell with LSM/YSZ cathode the reduction of the operating temperature is limited by a rapid increase of activation overvoltage and loss of performance, ohmic losses also increase but it is prevailing the limitation of lanthanum–strontium manganite based cathodes to work at intermediate temperature (750 °C). In the case of ASC2 cell the reduction of performance with the decrease of the temperature is less intense and arises mainly from the increase of ohmic resistivity and thus of ohmic losses.

2. Experimental

2.1. Experimental setup: polarization analysis

The tests were performed with circular shaped anode supported SOFC cells from InDEC®, with a diameter of 80 mm and an active area of 47 cm^2. The actual macroscopic geometrical features were determine from SEM of the cells.

The geometry and materials of the cells were

- (ASC1): anode 525–610 μm thick with two layers (both made of NiO/8YSZ cermet: functional layer 5–10 μm thick; support layer 520–600 μm thick); electrolyte 4–6 μm thick $Y_{0.16}Zr_{0.84}O_2$ (8YSZ), with unknown volume density; cathode 30–40 μm thick with two layers (functional layer of porous 8YSZ and $La_{0.75}Sr_{0.2}MnO_3$ (LSM); current collecting layer of LSM alone).
- (ASC2): anode 525–610 μm thick with two layers (both made of NiO/8YSZ cermet: functional layer 5–10 μm thick; support layer 520–600 μm thick); electrolyte 4–6 μm thick $Y_{0.16}Zr_{0.84}O_2$ (8YSZ), with unknown volume density; composite cathode consisting of a 2–4 μm thick barrier layer made of yttria doped ceria (YDC) and 20–30 μm thick functional layer made of porous lanthanum strontium cobalt ferrite oxide (LSCF). This second design allows the cell to be suitable for intermediate temperature operation.

The cells were tested in a ceramic cell housing consisting of alumina, with alumina flanges for gas distribution, platinum gauze for cathode current collection, and nickel gauze for anode current collection. The anode and cathode chambers were not sealed, allowing the fuel to react with oxygen directly outside the fuel cell. Platinum wires were used as current leads and for cell voltage measurement. For oxidant flow, oxygen and nitrogen were available.

For fuel flow, hydrogen and nitrogen mixtures were used. The fuel was humidified by a bubbler operating at 30 °C. The flows were controlled by mass flow controllers (Bronkhorst). Before tests, the cells were first stabilized at 736 °C under 3 A load (0.064 A cm^{-2}), with fuel consisting of 400 ml min^{-1} H_2 humidified at 30 °C and oxidant consisting of 1500 ml min^{-1} air (ml min^{-1} refers to normal conditions).

During the experimental session moisture was added to the fuel stream via saturation of the hydrogen flow at 30 °C corresponding to a water content of around 4%. The oxidant flow

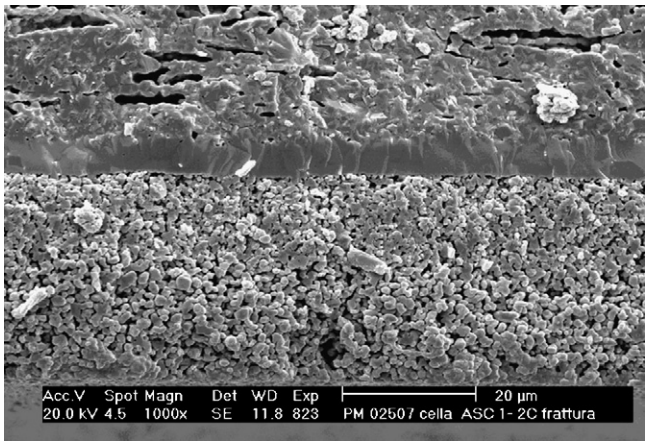

Fig. 1. Microscopy of ASC1 cell: comprehensive picture of the region close to the electrolyte.

consisted of 21% oxygen and 79% nitrogen, without water. Experiments were performed with high values of fuel utilization (maximum value around 0.77 at the highest current density), while the air was fed with very high excess with respect to the stoichiometric amount.

The *V–i* characteristics were taken changing current in steps of 1 A (0.021 A cm^{-2} for a time step of 60 s), by using a Kikusui electronic load (Kikusui Electronics Corp, Japan) in conjunction with an additional power supply in current-following mode (Delta Elektronica, Zierikzee, Netherlands). This additional power supply was needed because the electronic load was not able to control the low voltage output of the fuel cell.

2.2. Experimental setup: microscopy analysis

Concerning the microscopic analysis, a scanning electron microscopy (SEM) was used in order to analyze the microscopic topologies of the considered porous media. In particular, the energy dispersion spectroscopy (EDS) was adopted to distinguish different solid phases. The microscopic analysis was carried out by the research laboratory "Centro Ricerche Brasimone—ENEA" (Italy). The considered SEM was

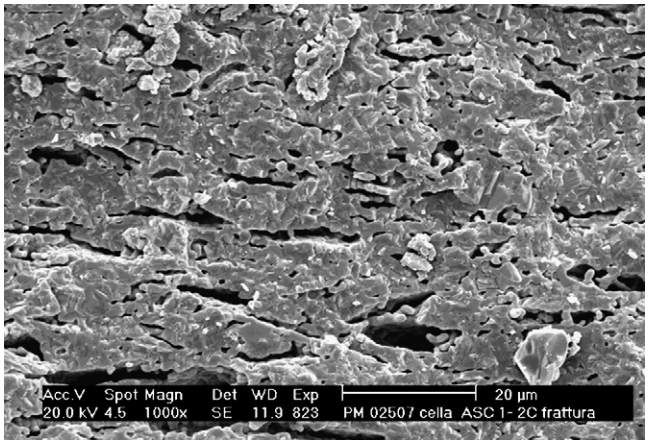

Fig. 2. Microscopy of ASC1 cell: detailed view of the anode region is reported.

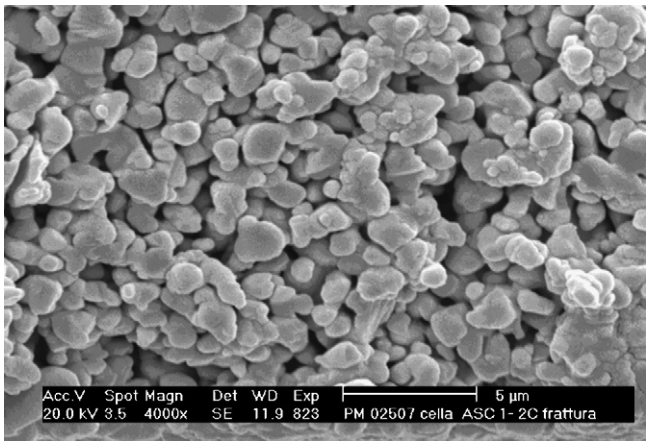

Fig. 3. Microscopy of ASC1 cell: detail concerning the cathode structure.

a PHILIPS XL 20, with a EDAX DX4—i module for the microanalysis.

The actual data about the dispersion of the solid phases were obtained by means of two detectors: the first for the morphological analysis involving the secondary electrons (SE) and the second for the atomic number contrast involving the backscattered electrons (BSE). The operative parameters for each microscopic picture (as indicated by the corresponding picture legend) are

- ACC.V acceleration voltage;
- SPOT characteristic length crossed by the electronic beam;
- MAGN adopted magnification;
- DET type of adopted detector (SE or BSE);
- WD working distance between the sample and the electron beam diaphragm.

An important issue in dealing with reliable microscopic analysis is the sample preparation. Complex sample preparations may lead to better quantitative information extracted by the samples, even though the latter may become more difficult to interpret. For this reason, both prepared and unprepared samples were considered in this analysis. The unprepared samples were

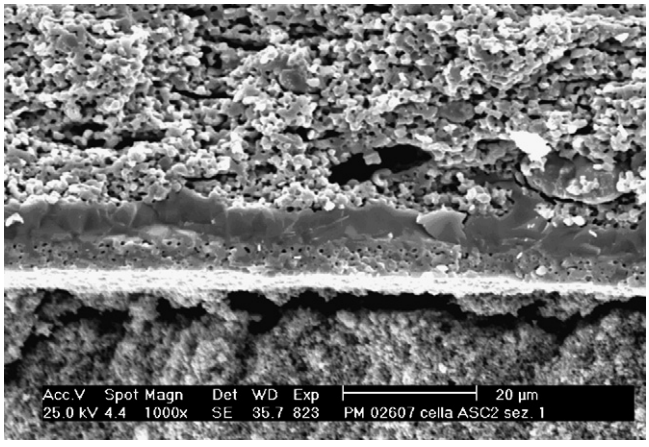

Fig. 4. Microscopy of ASC2 cell: comprehensive picture of the region close to the electrolyte.

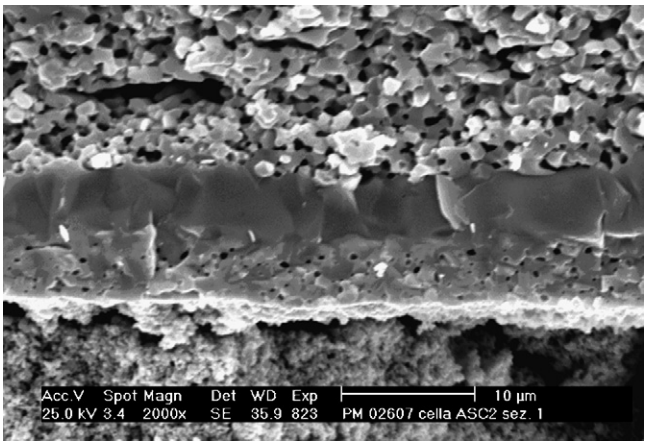

Fig. 5. Microscopy of ASC2 cell: detailed view of YDC barrier layer.

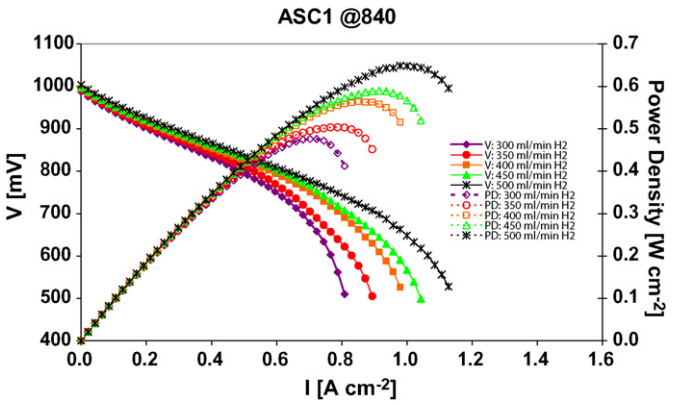

Fig. 7. Power-generating characteristics of unit-cells, anode supported cell with YSZ/LSM cathode (ASC1) at 840 °C.

simply obtained by regular fractures of the analyzed fuel cells. On the other hand, the prepared samples were submerged in conductive graphite or in epoxy resin, and subsequently polished by diamond grinding dish by means of an automatic polisher. Finally, in order to improve the quality of the corresponding SE pictures, some samples were coated by a thin gold layer (roughly 10 nm).

3. Microscopy of the cells

Fig. 1 reports a comprehensive picture of the region close to the ASC1 electrolyte, obtained by means of the scanning electronic microscope (SEM). All the pictures for ASC1 (Figs. 1–3) are related to an un-operated cell. For obtaining this picture, any preparation of the sample surface was avoided, in order to preserve the original structure of the porous media: for this reason, the cell was sharply broken in the investigated section. The result is much more effective in providing a qualitative description of the microscopic topology, but it cannot be used in order to perform accurate quantitative analysis (for example measuring the surface porosity), because different sections are involved in the reported picture. However, this representation is enough to catch the different structure of the anode and the cathode regions.

In particular, the anode is characterized by much larger pores, mainly stretched along the direction parallel to the electrolyte layer, while the cathode structure is much more isotropic. In Fig. 2 a detailed view of the anode region is reported, where the pore distribution clearly shows some self-similarities. It is worth the effort to point out that in this type of cells the anode must provide also the mechanical support for the whole cell. In Fig. 3 a detail concerning the cathode structure is reported with much higher magnification. This was done since the cathode is characterized by much smaller grains, which increase the degree of mixing. The previous consideration particularly holds for the functional layer, closer to the electrolyte, where most of the three-phase-boundaries (TPBs) are located.

Also the analysis was focused on the investigation of main microscopic features of ASC2 cell. Contrarily to the previous set of figures, all the pictures (Figs. 4–6) for ASC2 are related to the final structure after operation. This allows us to see the different structure in the anode layer due to the reduction of NiO to metallic Ni and the degradation of cathode side, leading to delamination of some portions. In Fig. 4 a comprehensive picture of the region close to the electrolyte is reported with the same magnification already used for the previous LSM-based cell. First of all, a simple comparison among the considered cells shows a much finer structure at the anode side for the second

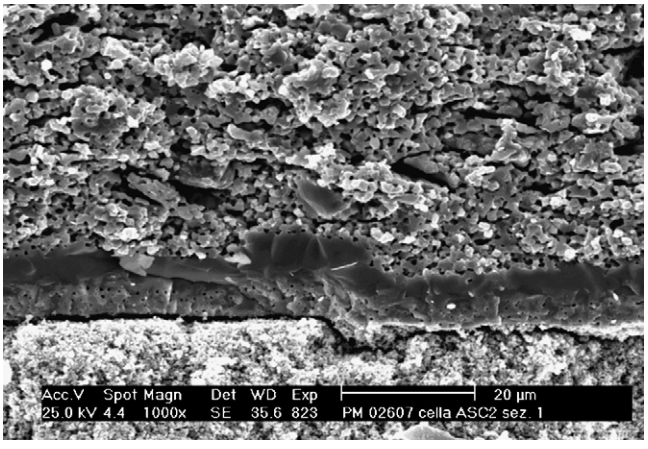

Fig. 6. Microscopy of ASC2 cell: detail of lack of planarity for both the electrolyte end barrier layer.

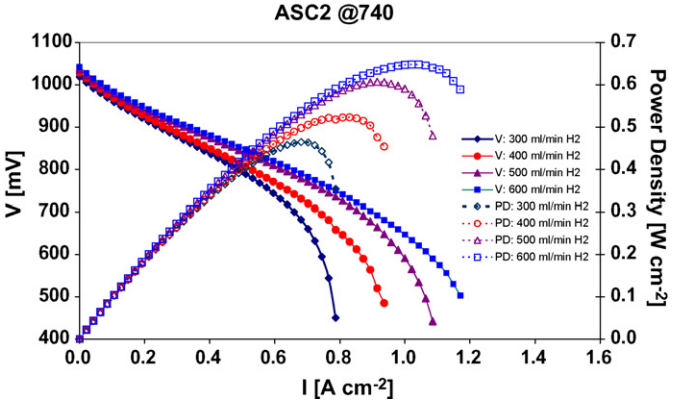

Fig. 8. Power-generating characteristics of unit-cells, anode supported cell with YDC/LSCF cathode (ASC2) at 740 °C.

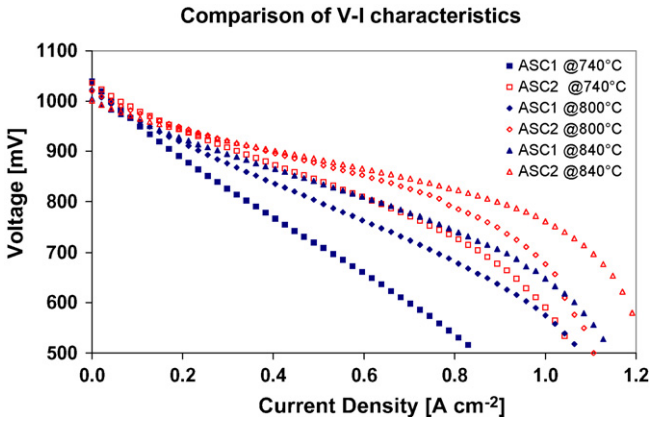

Fig. 9. Comparison of ASC1 and ASC2 performances.

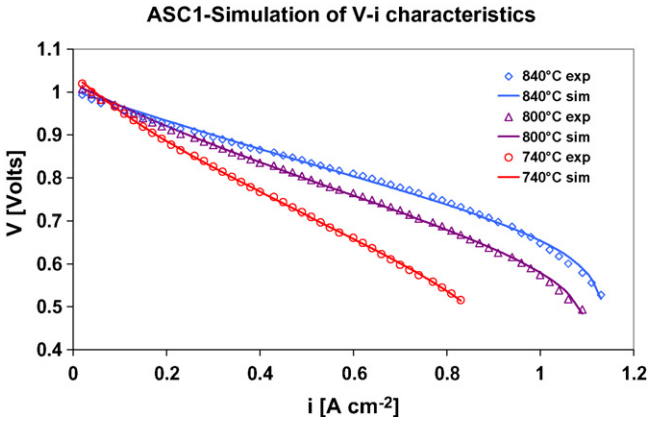

Fig. 11. Experimental vs. model behavior of anode-supported cell with LSM cathode.

LSCF-based cell, even though they both share the same anode composition. The reason is that the second type of cell is also the result of an improved manufacturing process, which allows one to reduce the grain size of first anodic layers at the electrolyte interface in order to achieve a larger active surface. The stretched pores are strongly reduced and some new micro-pores appear, leading to a more efficient topology, i.e. a topology characterized by a higher degree of mixing and dispersion among the different phases. Concerning the cathode side, in Fig. 5 a further magnification allows one to realize the existence of the YDC barrier layer, which is characterized by a very small porosity. This fundamental thin layer prevents undesired formation compounds at the interface of YSZ electrolyte and LSCF cathode by realizing a sort of chemical reaction barrier layer. In addition the YDC layer itself is chemically compatible with both YSZ and LSCF materials. This feature is particularly important during the manufacturing process, when the highest temperatures are achieved. From the mechanical point of view, the YDC layer allows one to match the different mechanical properties of YSZ electrolyte and LSCF cathode materials in terms of thermal expansion coefficients. The low porosity is not a problem because YDC must only transport the oxygen ions. However, some basic sample preparation was enough to damage the cathode functional layer. In fact in this section, the actual functional layer is missing, and what seems to replace it is actually another portion of it, more in-deep, which is out of focus. This is a simple consequence of the poor mechanical performances of this material. Finally in Fig. 6 a lack of planarity for both the electrolyte end barrier layer is shown. There is no evidence that this lack of planarity leads to performance worse than those due to the previous sections: in fact it seems that electrolyte is still continuous. Since this cell is an anode-supported the deposition of the cathode may compensate planarity defects in the electrolyte layer, anyway the need of good planarity for the total cell assembly is a fundamental feature for stack design.

4. Polarization behavior of the cells

4.1. Screening of cell performance

Aim of the paragraph is the comparison of cell performances as a function of the operating temperature (prior to the analysis of polarization limiting factors): the use of iron and cobalt-containing perovskites as cathodes for solid oxide fuel cells (SOFCs) allows one to decrease the operating temperature of around 100 °C without losses of performance with respect to state-of-the-art manganite-based perovskites. In Fig. 7 the measured *V–i* curves are drawn for the temperature of 840 °C for ASC1 cell, while in Fig. 8 results are reported for ASC2 cell at 740 °C. This condition leads to comparable performance of

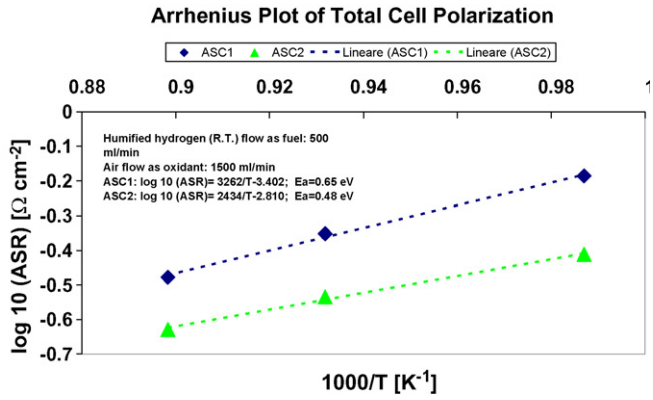

Fig. 10. Arrhenius plot of total cell resistance (ASR).

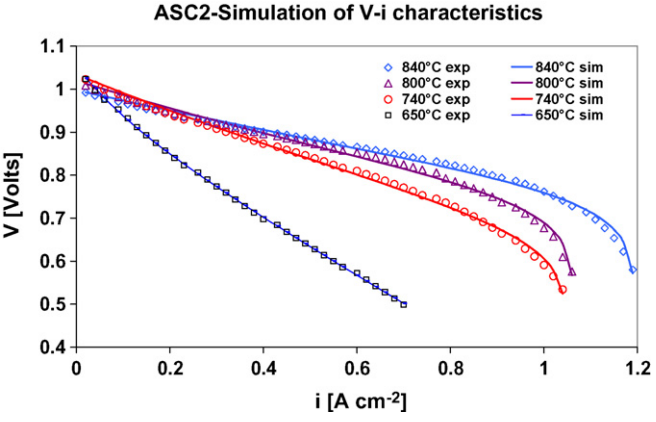

Fig. 12. Experimental vs. model behavior of anode-supported cell with LSCF cathode.

Table 1
Estimated parameters of polarization model for ASC1 and ASC2 cells

	ASC1 estimation	840 °C (Δ, confidence interval)	ASC2 estimation	840 °C (Δ, confidence interval)
$I_{0,c}$ (A cm^{-2})	0.197	±0.031	0.236	±0.045
R_Ω (Ω cm^2)	0.135	±0.013	0.048	±0.014
I_{as} (A cm^{-2})	1.144	±0.005	1.196	±0.002
	ASC1 Estimation	800 °C (Δ, confidence interval)	ASC2 estimation	800 °C (Δ, confidence interval)
$I_{0,c}$ (A cm^{-2})	0.112	±0.009	0.168	±0.032
R_Ω (Ω cm^2)	0.189	±0.008	0.081	±0.017
I_{as} (A cm^{-2})	1.113	±0.006	1.066	±0.002
	ASC1 estimation	740 °C (Δ, confidence interval)	ASC2 estimation	740 °C (Δ, confidence interval)
$I_{0,c}$ (A cm^{-2})	0.060	±0.003	0.147	±0.024
R_Ω (Ω cm^2)	0.322	±0.009	0.174	±0.014
I_{as} (A cm^{-2})	0.938	±0.020	1.050	±0.004
	ASC1 estimation	650 °C (Δ, confidence interval)	ASC2 estimation	650 °C (Δ, confidence interval)
$I_{0,c}$ (A cm^{-2})	NP	NP	0.041	±0.003
R_Ω (Ω cm^2)	NP	NP	0.508	±0.030
I_{as} (A cm^{-2})	NP	NP	1.275	±0.510

cells despite one hundred degrees of difference in temperature. In fact, the maximum power density (MPD) achieved was around 650 mW cm^{-2} for ASC1 cell (840 °C) and 610 mW cm^{-2} at 740 °C for the ASC2 cell.

The curves are traced for different fuel flow rates (and variable fuel utilization); at 0.5 A cm^{-2} the following fuel utilizations were achieved: 56.3% (300 ml min^{-1}), 47.8% (350 ml min^{-1}), 41.8% (400 ml min^{-1}), 37.2% (450 ml min^{-1}), 33.5% (500 ml min^{-1}), 30.7% (550 ml min^{-1}), 27.9% (600 ml min^{-1}).

In Fig. 9 *V–i* characteristics of ASC1 and ASC2 cells are drawn for 500 ml min^{-1} of hydrogen and for different operating temperatures. The current–voltage behavior of ASC2 at 740 °C is comparable with performance of ASC2 at 840 °C. In particular at 740 °C and 500 ml min^{-1} of fuel the voltage of 0.7 V is reached at around a double value of current density in the case of ASC2. Increasing the temperature the positive effect of the improved cathode decreases.

Also the cell performance was estimated in terms of the area specific resistance of the cell (ASR) [1,2,11]. This parameter can be assumed to be representative of total cell polarization. In this work the ASR was evaluated in the form of Eq. (1) [1]:

$$\mathrm{ASR} = \frac{\mathrm{OCV_{exp}} - V_c}{i} \quad (1)$$

where $\mathrm{OCV_{exp}}$ is the experimental open circuit voltage, V_c is the measured cell voltage and i the corresponding current density.

The following values of ASR were estimated for ASC1 at 500 ml min^{-1}: 0.65 Ω cm^2 at 740 °C, 0.44 Ω cm^2 at 800 °C, 0.33 Ω cm^2 at 840 °C. Concerning the ASC2 at 500 ml min^{-1}: 0.84 Ω cm^2 at 650 °C, 0.39 Ω cm^2 at 740 °C, 0.292 Ω cm^2 at 800 °C, 0.235 Ω cm^2 at 840 °C.

In Fig. 10 the Arrhenius plot of ASR is shown with the evaluated apparent thermal activation energies. The total cell resistance is less dependent on temperature in case of ASC2 than in case of ASC1. In fact the apparent activation energy related to total polarization was 0.65 eV for the cell with LSM/YSZ pair whereas it was 0.48 eV for the cell with LSCF cathode.

4.2. Electrochemical investigation of cell performance

In this paragraph the polarization analysis is refined describing a cell polarization model and fitting the experimental data through parameter estimation methods. In this way it has been possible to determine: (1) which terms of polarization is affected by the improved LSCF cathode and YDC barrier layer; (2) which is the contribution of single polarization terms to the total polarization; (3) which is the contribution of polarization terms to the performance variation with temperature; (4) which is the contribution of electrolyte, electrodes and contact resistance to the total ohmic losses.

4.2.1. Polarization model

The polarization analysis has been performed for the two cells, at different operating temperatures, fixed fuel mass flow of 500 ml min^{-1} (nominal condition) and fixed air mass flow of 1500 ml min^{-1}. The fuel was hydrogen with 4% of water, while the composition of the air was 21% oxygen 79% nitrogen without water. The *V–i* characteristics can be described according to a model which takes into account the main polarization terms: average Nernst potential, activation overvoltages, ohmic losses and diffusion losses. The cell voltage is expressed by Eq. (2):

$$V_c = V_{\mathrm{Nernst}} - \frac{RT}{\alpha F} a \sin h\left(\frac{i}{2I_{0,c}}\right) - R_\Omega i + \frac{RT}{2F}\log\left(1 - \frac{i}{i_{as}}\right) + \frac{RT}{4F}\log\left(1 - \frac{i}{i_{cs}}\right) \quad (2)$$

The Nernst potential, V_{Nernst}, has been assumed equal to the measured open circuit voltage.

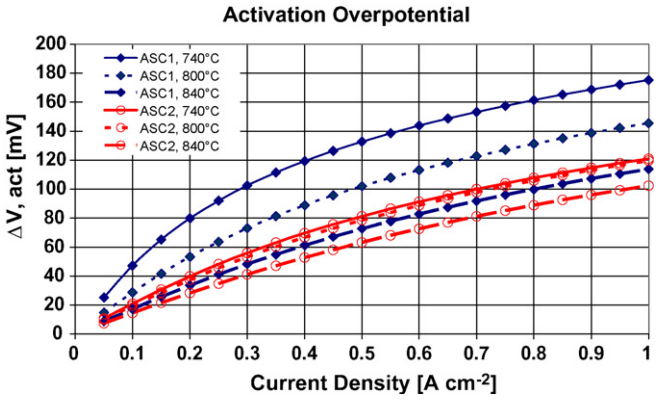

Fig. 13. Cathode activation overvoltages of ASC1 and ASC2 cells as function of temperature.

The activation overvoltage has been modeled using a single-term equation of the hyperbolic sine approximation of the Butler–Volmer equation. It is then assumed that one of the equilibrium exchange current densities is significantly larger than the other, thus allowing the corresponding activation loss to be neglected [24]. The coefficient α_{eff}, is the effective charge transfer coefficient, in the work it has been fixed at the value of 2, assumed from literature [25].

The ohmic resistance is modeled considering the resistance of electrolyte, electrodes, interface resistance and any contact resistance between current collectors. The resistance of 8YSZ electrolyte has been estimated using the resistivity expression in Eq. (3) [26,27]:

$$\rho_{\text{el}} = 0.00294\, e^{(10350/T_{\text{cell}})} \quad (3)$$

The concentration overvoltages are modelled considering the macroscopic concept of limiting current densities for both electrodes. Since both cells are anode supported, the anode limiting current densities will be estimated, while the diffusion overvoltage will be neglected at the very thin cathode side [5].

4.2.2. Parameter estimation

The current–voltage curves are analyzed using the polarization model of Eq. (2) and by statistical regression on the experimental data. Parameter estimation method was used in order to break-down the main contribution of the polarization resistance of the cell. The estimation of parameters was accomplished using the Levenberg–Marquardt algorithm which interpolates between the Gauss–Newton algorithm and the method of gradient descent. The former algorithm is more robust than the latter one, which means that in many cases it finds a solution even if it starts very far off the final minimum. The quality of estimates is judged by means of 95% confidence intervals. Three parameters have been estimated in the analysis, (1) the cathode exchange current densities $I_{0,c}$, (2) the ohmic resistance R_Ω and (3) the anode limiting current density i_{as}. In Figs. 11 and 12 the results of the estimation procedure are drawn with experimental and model V–i curves. The values of the estimated parameter are reported in Table 1.

The ohmic polarization is temperature dependent mainly because the thermally activated dependence of the 8YSZ ionic resistivity, with exponential behavior such the one expressed in Eq. (3): therefore, also the ohmic resistance decreases at the increase of temperature with exponential behavior.

The activation polarization is also thermally activated, which is reflected in the thermally activated dependence of the exchange current density $I_{0,c}$: in fact the cathode exchange current densities increase at the increase of temperature with meaning of reduction of electrode polarization at high temperature.

Anode limiting current densities slightly varies with temperature as expected. Further, with decreased temperature worst estimations of anode limiting current densities were obtained (the confidence domain of parameter is defined with higher uncertainty), suggesting that at low temperature other sources of polarization, rather than concentration, limit the cell performance.

Thus, the principal temperature dependence of cell performance is due to the temperature dependence of ohmic and activation polarization. In the next paragraph, it will be outlined that performance limitation at low temperature is due to activation polarization for ASC1 and ohmic polarization for ASC2.

Table 2
Area specific resistance (ASR), ohmic contribution to polarization of ASC1 cell

G_{H2} (N ml min^{-1})	σ_{YSZ} (S cm^{-1})	R_{YSZ} (Ω cm^2)	R_Ω (Ω cm^2)	ASR (Ω cm^2)	R_{YSZ}/R_Ω (%)	R_Ω/ASR (%)
740 °C						
500	1.2E-02	4.8E-02	0.322	0.652	15.0	49.4
600	1.2E-02	4.8E-02	0.322	0.658	15.0	48.9
800 °C						
300	2.2E-02	2.7E-02	0.189	0.492	14.4	38.4
400	2.2E-02	2.7E-02	0.189	0.452	14.4	41.8
500	2.2E-02	2.7E-02	0.189	0.445	14.4	42.5
840 °C						
300	3.1E-02	1.9E-02	0.135	0.384	14.3	35.2
350	3.1E-02	1.9E-02	0.135	0.364	14.3	37.1
400	3.1E-02	1.9E-02	0.135	0.341	14.3	39.6
450	3.1E-02	1.9E-02	0.135	0.329	14.3	41.0
500	3.1E-02	1.9E-02	0.135	0.333	14.3	40.5

Table 3
Area specific resistance (ASR), ohmic contribution to polarization of ASC2 cell

G_{H2} (N ml min^{-1})	σ_{YSZ} (S cm^{-1})	R_{YSZ} (Ω cm^2)	R_Ω (Ω cm^2)	ASR (Ω cm^2)	R_{YSZ}/R_Ω (%)	R_Ω/ASR (%)
650 °C						
400	4E-03	1.31E-01	0.508	0.844	25.8	60.2
500	4E-03	1.31E-01	0.508	0.842	25.8	60.3
600	4E-03	1.31E-01	0.508	0.76	25.8	66.8
740 °C						
300	1.2E-02	4.8E-02	0.174	0.45	27.7	38.7
400	1.2E-02	4.8E-02	0.174	0.437	27.7	39.8
500	1.2E-02	4.8E-02	0.174	0.388	27.7	44.8
600	1.2E-02	4.8E-02	0.174	0.386	27.7	45.1
800 °C						
300	2.2E-02	2.7E-02	0.081	0.333	33.6	24.3
400	2.2E-02	2.7E-02	0.081	0.309	33.6	26.2
500	2.2E-02	2.7E-02	0.081	0.292	33.6	27.7
600	2.2E-02	2.7E-02	0.081	0.288	33.6	28.1
840 °C						
300	3.1E-02	1.9E-02	0.048	0.274	40.2	17.5
400	3.1E-02	1.9E-02	0.048	0.26	40.2	18.5
500	3.1E-02	1.9E-02	0.048	0.235	40.2	20.4

At 800 °C values of cathode exchange current densities of around 110 and 170 mA cm^{-2} were found for ASC1 and for ASC2, respectively. Basing on the concept of effective charge transfer resistance [28,29], the effective exchange current density can be related with the effective charge transfer resistance of the two cells.

The commonly used equation of Butler–Volmer, which defines the activation overpotentials at an electrode, can be expressed with the hyperbolic sine approximation with a very low error. However, at low current densities (approximately up to the value of the exchange current density) the activation polarization can be also approximated as being ohmic (linear with current). This linear approximation is derived expanding in a power series the Butler–Volmer equation and neglecting the higher order and all the non-linear terms. It is so introduced an effective charge transfer resistance, R_{ct}^{eff}, which is defined in term of various parameters, including the intrinsic charge transfer resistance, R_{ct}, which is a characteristic of the electrocatalyst/electrolyte pair (LSM/8YSZ) and also depends on TPBL, and the electrode thickness. It is known that the effective charge transfer resistance, R_{ct}^{eff}, reaches an asymptotic with the increase of electrode thickness. The limiting value of the effective charge resistance depends on the magnitude of the ionic conductivity of the composite electrode, σ_{8YSZ}, the intrinsic charge transfer resistance, R_{ct} and the grain size of the electrolyte in the electrode, B [28,29]:

$$R_{ct}^{eff} = \frac{BR_{ct}}{B((1+\beta)/(1+\beta e^{(-2h/\lambda)}))(1-\varepsilon)e^{(h/\lambda)} + ((1+\beta e^{(-h/\lambda)})/(1+\beta e^{(-2h/\lambda)}))\lambda(1-e^{(-h/\lambda)}) + B\varepsilon} \ (\Omega\,cm^2) \quad (4)$$

and

$$\lambda = \sqrt{\sigma_{8YSZ} B(1-\varepsilon)R_{ct}} \qquad \beta = \frac{\sigma_{8YSZ}R_{ct} - \lambda}{\sigma_{8YSZ}R_{ct} + \lambda} \quad (5)$$

The main hypothesis of the model are (i) the electronic resistance of the electrocatalyst is negligible;(ii) the oxygen ion conductivity of electrolyte is assumed to be independent of position, in fact, the oxygen ion conductivity of electrolyte is known to be mainly a function of the local oxygen pressure and thus of position; (iii) the effect of concentration is polarization is significant only at high current densities, it is thus assumed that partial pressures of gases are constant; (iv) it is assumed that activation overpotential is ohmically related to the local current density at the electrocatalyst–electrolyte interface through R_{ct}.

For the analyzed condition, values of effective charge transfer resistance of around 0.2 Ω cm^2 for ASC1 and 0.13 Ω cm^2 for ASC2 have derived at 800 °C. In particular, the estimation for the cell with LSM/YSZ electrocatalyst/electrolyte pair is in accordance with other works in literature and correspond to a cathode functional layer with porosity of around 20–25%, grain size of around 1–2 μm (Fig. 3), ionic conductivity of around 0.02 S cm^{-1} and thickness of around 15–20 μm.

In Table 2 the estimated ohmic resistances are compared with the ionic resistance of electrolyte. In general, the estimated values are higher than values of ionic resistance of electrolyte: this means that there is an important contribution of ohmic resistance which arises from other sources such as electrode resistance, resistance of interfaces, contact resistance. In particular, the contribution of the electrode resistance can strongly affect the cell performance in case of the ASC1 cell.

Anode limiting current densities slightly varies for the two investigated cells. Concentration overvoltages evaluated in this analysis are strongly dependent with operating condi-

tions and include contribution of conversion resistance (fuel utilization).

5. Polarization limiting performance factors of cells

5.1. Polarization analysis

In Fig. 13 the activation overvoltage of the electrochemical reaction at the cathode side is drawn. As expected from results obtained by the literature overview on the topic, ASC2 has lower activation overvoltage because LSCF cathode enhances the medium-temperature performance adding a second ionically conducting phase and thus extending the surface area over which the oxygen reduction reaction can occur. In particular, activation overvoltage of ASC2 seems less dependent on temperature at least in the range investigated in the work (740–840 °C).

In Tables 2 and 3 the contribution of electrolyte resistance to the total ohmic resistance, and of the ohmic resistance to the total ASR, are shown. In the case of ASC1 cell, the values of R_{YSZ}/R_{Ω} ratio are lower than the ones obtained for the ASC2 cell. At 740 °C it was estimated a contribution of electrolyte resistance to ohmic resistance of around 15% for ASC1 and 28% for ASC2 cells, respectively. This means that ASC2 cell had reduced electrode resistance and eventual ohmic resistance of interfaces.

Higher values of R_{Ω}/ASR ratio were found in case of ASC1 cell: in fact, at 740 °C and 500 ml min^{-1} of fuel, the contribution of ohmic to total cell resistance was 49.4% whereas for ASC2 cell it was 44.8%; the value of the ohmic resistance is almost halved with LSCF cathode (0.322 Ω cm^2 for ASC1 versus 0.174 Ω cm^2 for ASC2).

In both cases the contribution of the electrolyte accounts for a small part even at intermediate temperature: this means that YSZ can work as electrolyte in this design of cells for intermediate temperature operation (700–750 °C) and that it is not necessary to try to reduce further its thickness [6]. So our analysis helped to clarify that is more convenient to focus on the cathode electrode improvement rather than seeking for better electrolyte materials in terms of ionic conductivity or developing techniques to produce thinner layers at least in the range of investigated temperatures (intermediate temperature range).

5.2. Thermal activated process analysis

A comparison of cell behavior in terms of polarization and effect of temperature has been done. In fact, the apparent thermal activation energy E_a has been evaluated from the temperature dependence of ASR given in Tables 2 and 3. In Fig. 10 the Arrhenius plot of ASR is shown with the evaluated apparent thermal activation energies.

The cell with LSCF cathode has a lower activation energy and it is possible to conclude that this cell is suitable for operating at reduced temperatures compared to the ASC1 cell. In particular, for the ASC1 cell an apparent thermal activation energy of around 0.65 eV has been estimated, while for the ASC2 cell a value of E_a of around 0.48 eV has been evaluated. The difference of the estimated values of thermal activation energy

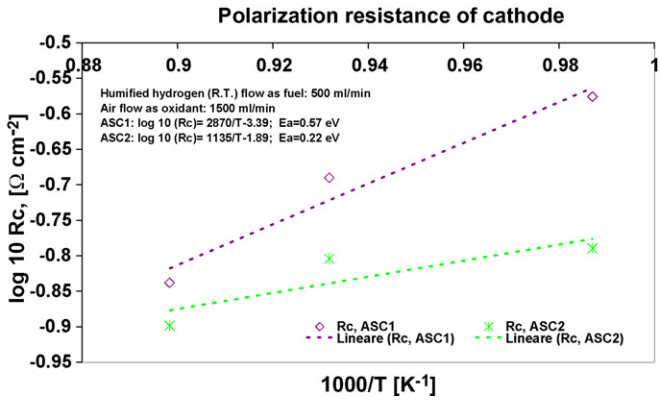

Fig. 14. Arrhenius plot of cathode resistance.

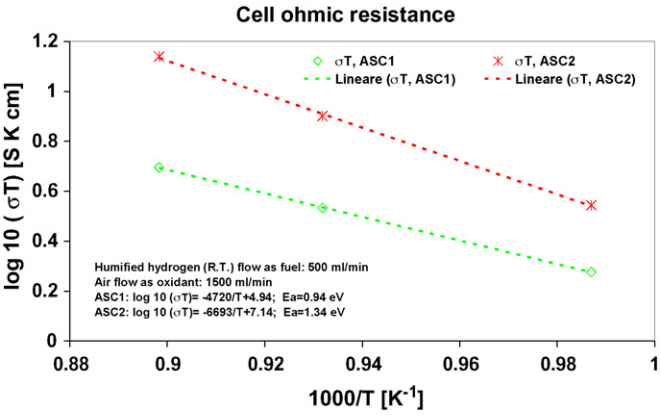

Fig. 15. Arrhenius plot of ohmic resistance.

means that the two tested cells have different thermally activated electrochemical performances which are related to the different material employed in the cathode electrode. In particular the ASC1 cathode material has electrical and electrochemical properties highly depending on the operating temperature and fast degrading as it goes below 800 °C.

In Figs. 14 and 15 the Arrhenius plot of the cathode polarization resistance (evaluated as the ratio between activation overvoltage at 0.5 A cm^{-2} and current of 0.5 A cm^{-2}) and of the ohmic resistance are shown.

The E_a, referred to the polarization resistances at cathode, of ASC1 is higher than the ASC2 one. This means that for the ASC1 cell the activation polarization term is the limiting factor when lowering the operating temperature. This suggest a modification of the cathode material and structure (inclusion of an interface layer, increase of the cathode thickness, modification of the grain size, etc.).

The E_a, referred to the ohmic resistances, of ASC1 is lower than the ASC2 one. This means that for the ASC2 cell the ohmic polarization is the limiting factor when lowering the operating temperature. This suggests that for reducing effectively the operating temperature of the ASC2 below 700 °C other materials for the electrolyte layer should be taken into account (other than 8YSZ).

However, also the need for a more conducting electrolyte to reduce the temperature below 700 °C does not seems crucial

from the results of our analysis. Since we considered electrode-supported cells and the electrolyte thickness is already much reduced, it appears that the ohmic contribution to total polarization is not dominated from the 8YSZ ohmic resistance. To lower further the working temperature, it seems more important that new and improved cathode materials should be employed with better electrical and electrochemical performances. The electrodes' design optimization (granulometry, porosity, thickness) could be also useful in having good performances even at low temperatures.

6. Conclusions

In this paper an analysis of solid oxide fuel cell performance was performed and was focused on the comparison of behavior of two anode supported cells with LSM (ASC1) and LSCF (ASC2) cathodes. The main results of the analysis were

- the maximum power densities (MPD) of ASC1 cell was ~649.0 mW cm^{-2}, at 840 °C and 500 ml min^{-1} of fuel. At the same operating condition for ASC2 cell was obtained ~775 mW cm^{-2}.
- the current–voltage behavior of ASC2 at 740 °C is comparable with performance of ASC2 at 840 °C; at 740 °C and 500 ml min^{-1} of fuel the voltage of 0.7 V is reached at a double value of current density in the case of ASC2.
- ASC2 has lower activation overvoltage because LSCF cathode enhances the medium-temperature performance adding a second ionically conducting phase and thus extending the surface area over which the oxygen reduction reaction can occur.
- at 800 °C values of cathode exchange current densities of around 110 mA cm^{-2} for ASC1 and 170 mA cm^{-2} for ASC2 were found; the effective charge transfer resistance estimated values were around 0.2 Ω cm^2 for ASC1 and 0.13 Ω cm^2 for ASC2; the estimation for the cell with LSM/YSZ electrocatalyst/electrolyte pair is in accordance with other works in literature and correspond to an optimized cathode functional layer.
- the ohmic contribution is almost halved with the improved design of LSCF cathode: this can be due to the reduction of electrode resistance and better current collection at cathode side. The LSCF, in fact, is itself a good electronic-collector material and it is directly placed in contact with the Pt mesh.
- the E_a referred to the ohmic resistances is lower for ASC1; the referred to the cathode polarization resistances is lower for ASC2; therefore, when reducing the operation temperature the activation polarization term is the limiting factor for ASC1, while the ohmic polarization term is the limiting factor for ASC2.
- pointing at working in an intermediate temperature range, for the ASC1 cell the limiting factor is represented by the cathode polarization in accordance to the E_a estimated for the LSM/8YSZ composite electrode; the cathode polarization E_a is indeed much lower for the ASC2 cell.
- the limiting factor to obtain better performances from the ASC2 cell is represented by the ohmic polarization according to Fig. 15; anyway, the 8YSZ electrolyte resistance seems to be not the dominant term of total ohmic resistance of the cell: to lower further the working temperature, it seems more important that new and improved cathode materials should be employed with better electrical and electrochemical performances.

Acknowledgements

The authors would like to thank Dr. Andrea Ciampichetti and Massimo Agostini of "Centro Ricerche Brasimone—ENEA" for providing the SEM images.

References

[1] T.M. Koehler, D.B. Jarrel, L.J. Bond, High temperature ceramic fuel cell measurement and diagnostics for application to solid oxide fuel cell systems, Report prepared for the U.S. Department of Energy, October 2001.
[2] S.C. Singhal, K. Kendall, High Temperature Solid Oxide Fuel Cells: Fundamentals, Design and Applications, Elsevier, 2004.
[3] S. Gopalan, G. DiGiuseppe, J. Power Sources 125 (2004) 183–188.
[4] K. Huang, Proceedings of the 7th European SOFC Forum, Lucerne (Switzerland), July 3–7, 2006.
[5] J. Kim, A.V. Virkar, K.Z. Fung, K. Metha, S.C. Singhal, J. Electrochem. Soc. 146 (1) (1999) 69–78.
[6] F. Zhao, A.V. Virkar, J. Power Sources 141 (2005) 79–95.
[7] N. Bessette, D.S. Schmidt, J. Rawson, R. Foster, A. Litka, Technical Progress Report Semi Annual, Acumentrics Advanced Power & Energy Technologies, February 2006.
[8] A. Gubner, T. Nguyen-Xuan, M. Bram, J. Remmel, L.G.J. de Haart (Bert), Proceedings of the 7th European SOFC Forum 2006, Lucerne, July 3–5, 2006.
[9] M. Lang, C. Auer, A. Eismann, T. Franco, C. Lachenmann, G. Schiller, P. Szabo, Proceedings of the 7th European SOFC Forum 2006, Lucerne, July 3–5, 2006.
[10] M. Santarelli, P. Leone, M. Calì, G. Orsello, J. Power Sources 171 (2007) 155–168.
[11] H.Y. Jung, W.-S. Kim, S.-H. Choi, H.-C. Kim, J. Kim, H.-W. Lee, J.-H. Lee, J. Power Sources 155 (2006) 145–151.
[12] V.V. Srdic, R.P. Omorjan, J. Seidel, Mater. Sci. Eng. B 116 (2005) 119–124.
[13] V. Dusastre, J.A. Kilner, Solid State Ionics 126 (1999) 163.
[14] A. Mai, V.A.C. Haanappel, S. Uhlenbruck, F. Tietz, D. Stover, Solid State Ionics 176 (2005) 1341–1350.
[15] T. Yang Chih-Chung, J. Wei Wen-Cheng, A. Roosen, Mater. Chem. Phys. 81 (2003) 134–142.
[16] M. Mogensen, N.M. Sammes, G.A. Tompsett, Solid State Ionics 129 (2000) 63–94.
[17] F. Tietz, V.A.C. Haanappel, A. Mai, J. Mertens, D. Stover, J. Power Sources 156 (2006) 20–22.
[18] E.P. Murray, M.J. Sever, S.A. Barnett, Solid State Ionics 148 (2002) 27–34.
[19] H.Y. Tu, Y. Takeda, N. Imanishi, O. Yamamoto, Solid State Ionics 117 (1999) 277–281.
[20] O. Yamamoto, Y. Takeda, R. Kanno, M. Noda, Solid State Ionics 22 (1987) 241–246.
[21] S.P. Jiang, W. Wang, Solid State Ionics 176 (2005) 1351–1357.
[22] T. Tsai, S.A. Barnett, Solid State Ionics 98 (1997) 191–196.
[23] B. Rietveld, Low Temperature SOFC for lifetime and reduced costs, Finnish SOFC Symposium, June 29, 2006.
[24] D.A. Noren, M.A. Hoffman, J. Power Sources 152 (2005) 175–181.
[25] P. Costamagna, K. Honegger, J. Electrochem. Soc. 145 (11) (1998) 3995–4006.

[26] L. Baozhen, R. Ruka, S.C. Singhal, Solid oxide fuel cell operable over wide temperature range, US Patent no. 6,207,311 B1, Inventors Assigne: Siemens Westinghouse Power Corporation, March 27, 2001.
[27] I.I.N.F. Bessette, W.J. Wepfer, J. Winnick, J. Electrochem. Soc. 142 (1995) 3792–3800.
[28] A.V. Virkar, J. Chen, C.W. Tanner, J.-W. Kim, Solid State Ionics 131 (2000) 189–198.
[29] C.W. Tanner, K.-Z. Fung, A.V. Virkar, J. Electrochem. Soc. 144 (1) (1997) 21–30.